

Thermo-Fluidodynamical Modelling of Laser Beam-Matter Interaction in Selective Laser Melting

K.-H. Leitz^{1*}, P. Singer¹, A. Plankensteiner¹, B. Tabernig¹, H. Kestler¹, L.S. Sigl¹

¹Plansee SE, Metallwerk-Plansee-Straße 71, 6600 Reutte, Austria

*Corresponding author: karl-heinz.leitz@plansee.com

Abstract: Selective Laser Melting (SLM) offers great potential for future manufacturing technology. In order to extend its applicability for the processing of high melting materials like molybdenum fundamental process understanding is required. This can be obtained by multi-physical simulations that allow a look into the process. In this contribution a thermo-fluidodynamical simulation model for laser beam-matter interaction based on *Comsol Multiphysics* is presented and applied for an analysis of the SLM process. The model includes the absorption of laser radiation, conductive and convective heat transfer as well as melting, solidification, evaporation and condensation processes. Based on the model a material specific comparison of SLM of steel and molybdenum is performed. Whereas for steel a long melt pool and a significant amount of evaporation is found, for molybdenum the melt pool is restricted to the size of the laser beam and no evaporation is observed.

Keywords: Selective Laser Melting, laser beam-matter interaction, molybdenum, steel

1. Introduction

In Selective Laser Melting (SLM) a laser beam is applied to build up a workpiece by melting up powder layer by layer (see Figures 1 a and b). The technology offers great potential for future manufacturing technology, as it allows unique design possibilities at short process chains and small lot sizes [1]. Whereas for materials like aluminum, steel, titanium, nickel and cobalt chromium alloys SLM is already well established and commercial fabrication systems are available, its application for the processing of high melting metals like molybdenum requires a fundamental process understanding as the processing window is significantly narrower. Nevertheless, SLM of molybdenum is feasible and promising results already can be achieved. Figure 1 c shows

molybdenum demonstrator parts that have been fabricated by SLM at Plansee SE.

In order to further extend the applicability of SLM for the processing of refractory metals, multi-physical simulations are a versatile tool. They allow a look into the process, to identify relevant process parameters and to develop a fundamental process understanding.

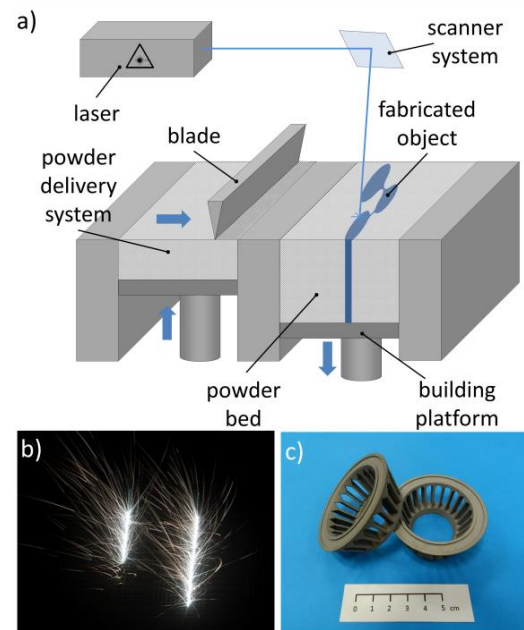


Figure 1. Selective Laser Melting: a) technology principle; b) process during operation; c) molybdenum demonstrator parts fabricated at Plansee SE.

However, modelling of laser beam-matter interaction is a challenging task, as it requires a coupled thermo-fluidodynamical description of the absorption of laser radiation, conductive and convective heat transfer, phase transition and wetting processes. Approaches for such a multi-physical modelling of laser beam-matter interaction on a mesoscopic scale have been developed for a variety of laser processes [2–6] including SLM [7, 8]. At Plansee SE a thermo-fluidodynamical model for laser beam-matter interaction based on those approaches was

developed and applied for an analysis of SLM of refractory metals. In the following the simulation model and its implementation in *Comsol Multiphysics* shall be described in detail.

2. Simulation Model

The multi-physical simulation model for laser beam-matter interaction in SLM includes the absorption of laser radiation on the surface of the metal powder, conductive and convective heat transfer in the metal and the ambient atmosphere as well as melting, solidification, evaporation and condensation processes. It uses a coupled thermo-fluidodynamical description of metal and ambient atmosphere based on the phase field approach. Depending on the temperature, the actual two-phase description distinguishes between solid, liquid and vapor phase state within the metal phase. The solid is treated as a high viscous fluid and the surface tension is restricted to the liquid phase. The density change during evaporation is taken into account based on an approach described in [12].

The simulation model for laser beam-matter interaction respectively SLM is based on the *Computational Fluid Dynamics* and the *Heat Transfer* module of *Comsol Multiphysics*. The model geometry consists of a simple cubic arranged metal powder layer (particle size $d_{part} = 40 \mu\text{m}$) on a massive base plate ($d_{plate} = 100 \mu\text{m}$) in air atmosphere irradiated by a Gaussian laser beam ($d_{focus} = 130 \mu\text{m}$).

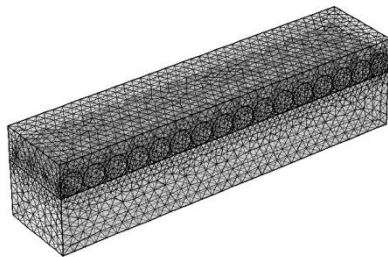


Figure 2. Finite element mesh.

The FE-mesh applied for the simulation consists of 116002 tetrahedral elements with a characteristic size of $5 \mu\text{m}$ in the particle layer and $20 \mu\text{m}$ in the boundary regions, respectively.

It is shown in Figure 2. The model makes use of symmetry along the direction of laser movement.

The thermal calculation in the model is based on the *Heat Transfer in Fluids* interface. The heat conduction equation

$$\rho \tilde{c}_p \frac{\partial T}{\partial t} + \rho \tilde{c}_p \mathbf{u} \cdot \nabla T = \nabla \cdot (k \nabla T) + \Gamma_{top} A Q_{Laser} - \Gamma Q_{rad} \quad (1)$$

implemented there, with the density ρ [kg/m^3], the effective heat capacity \tilde{c}_p [J/kg], the velocity \mathbf{u} [m/s] and the thermal conductivity k [$\text{W}/(\text{m} \cdot \text{K})$] describes the formation of the temperature field T [K] due to the energy input by the laser. The interface function Γ [$1/\text{m}$] is defined to be one for all elements at the metal-air interface. The energy input is implemented as a volume heat source. It is assumed, that the intensity Q_{Laser} [W/m^2] of the laser is absorbed with an absorption coefficient A [$-$] on the top surface Γ_{top} [$1/\text{m}$] of the metal.

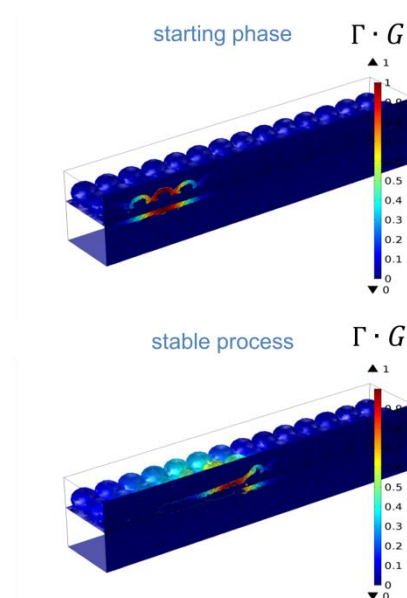


Figure 3. Normalized energy input at different process stages (Γ [$1/\text{m}$]: interface function; $G = Q_{Laser}/Q_{Laser,max}$: normalized Gaussian intensity distribution).

Figure 3 shows the normalized energy input at different process stages. Angle dependency of the absorption, shadowing effects and multiple reflections are neglected. These simplifications

are justified, as in the starting phase of the process neglecting shadowing approximates the increased energy input to the substrate due to multiple reflections in the powder bed. In a later process phase the laser energy is absorbed on the more or less smooth melt pool surface. This justifies the neglect of the angle dependency of absorbance. Furthermore, thermal radiation losses on the metal surface Γ [1/m] according to Stefan-Boltzmann law are considered by a heat sink Q_{rad} [W/m²]. The latent heats of melting H_m [J/kg] and evaporation H_v [J/kg] are taken into account by an effective heat capacity $\tilde{C}_p = C_p + \delta(T - T_m)H_m + \delta(T - T_v)H_v$ [J/(kg·K)] based on the *Heat Transfer with Phase Change* feature. T_m [K] and T_v [K] are melting respectively evaporation temperature. To model the building platform for the outer plate boundaries a temperature of $T_0 = 293$ K is prescribed.

The multi-phase fluid mechanical description uses the *Laminar Two-Phase Flow Phase Field* interface based on the Navier-Stokes equation, the continuity equation and the Cahn-Hilliard equation.

The Navier-Stokes equation

$$\rho \frac{\partial \mathbf{u}}{\partial t} + \rho(\mathbf{u} \cdot \nabla)\mathbf{u} = -\nabla p + \mu \nabla^2 \mathbf{u} + \rho \mathbf{g} + \mathbf{F}_\sigma \quad (2)$$

with the velocity \mathbf{u} [m/s], the pressure p [N/m²], the viscosity μ [Pa·s], the gravity constant \mathbf{g} [m/s²] and the surface tension force \mathbf{F}_σ [N/m³] describes the fluid mechanics of the system. Depending on the temperature in the metal phase it is distinguished between solid, liquid and vapor phase state. The solid phase is described as a high viscous fluid with the velocity constrained to zero. In addition to that the surface tension is restricted to the liquid phase.

The incompressible continuity equation

$$\nabla \cdot \mathbf{u} = Q_v \quad (3)$$

with the velocity \mathbf{u} [m/s] assures the conservation of mass. It includes a source term

$$Q_v = \dot{m} \cdot \Gamma \cdot \left(\frac{1}{\rho_{vap}} - \frac{1}{\rho_{met}} \right) \quad [1/s] \quad (4)$$

with the evaporation rate \dot{m} [kg/(m²·s)], the vapour density ρ_{vap} [kg/m³] and the metal density ρ_{met} [kg/m³] accounting for the density change during evaporation on the metal surface Γ [1/m]. The vapor density ρ_{vap} [kg/m³] is calculated on the base of the ideal gas law. In order to account for the fact that the mesh size h [m] cannot resolve the Knudsen layer that has an extend of the mean free path length of the vapor atoms (compare Figure 4) [9, 10]

$$l_{Knud} = \frac{k_B T}{\sqrt{2} \pi d^2 \cdot p_{vap}}, \quad (5)$$

a correction factor of h/l_{Knud} [-] is introduced:

$$\rho_{vap} = \frac{h}{l_{Knud}} \cdot \frac{M}{RT} \cdot p_{vap}. \quad (6)$$

In these relations k_B [J/K] is Boltzmann's constant, d [m] the atom diameter, h [m] the element size, M [kg/mol] the molar mass and R [J/(mol·K)] the ideal gas constant. The vapor pressure p_{vap} [N/m²] is given by [DEM01]

$$p_{vap} = p_0 \cdot \exp\left(\frac{H_v M}{R} \cdot \left(\frac{1}{T_v} - \frac{1}{T}\right)\right) \quad (7)$$

with the evaporation enthalpy H_v [J/kg] and the evaporation temperature T_v [K].

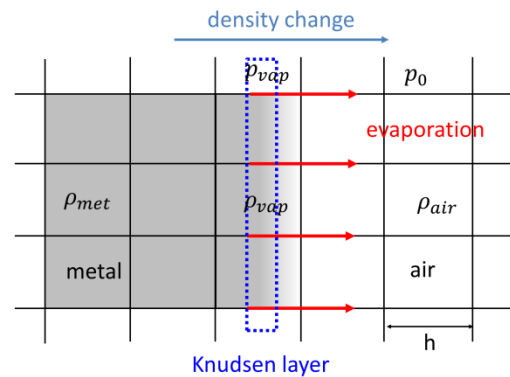


Figure 4. Evaporation modelling.

The evaporation rate \dot{m} [kg/(m²·s)] is calculated on the base of the Hertz-Knudsen formula [11]

$$\dot{m} = \varphi_{vap} \cdot (p_{vap} - p_0) \cdot \sqrt{\frac{M}{2\pi RT}} \quad (8)$$

with the vapor phase fraction φ_{vap} [-]. For the calculation an ambient pressure of $p_0 = 1$ bar is assumed.

The multi-phase description is based on the Cahn-Hilliard equation for the phase function Φ [-]

$$\frac{\partial \Phi}{\partial t} + \mathbf{u} \cdot \nabla \Phi = \nabla \cdot \frac{\gamma \lambda}{\varepsilon^2} \psi + Q_v' \quad (9)$$

$$\psi = -\nabla \cdot \varepsilon^2 \nabla \Phi + (\Phi^2 - 1)\Phi \quad (10)$$

with the mobility γ [(m · s)/kg], the mixing energy density λ [N], the surface tension coefficient σ [N/m] and the capillary width $\varepsilon = 2\sqrt{2} \cdot \lambda / (3 \cdot \sigma)$ [m]. The source term

$$Q_v' = \dot{m} \cdot \Gamma \cdot \left(\frac{1 - \Phi}{\rho_{vap}} + \frac{\Phi}{\rho_{met}} \right) [1/s] \quad (11)$$

accounts for the evaporation process.

The source terms Q_v [1/s] and Q_v' [1/s] for evaporation in continuity and Cahn-Hilliard equation are implemented as *weak contributions* in the *Laminar Two-Phase Flow Phase Field* interface.

3. Simulation Results

Based on the model a material specific comparison of SLM of stainless steel (1.4404) and molybdenum was performed. Temperature dependent material properties were taken from the *Comsol Multiphysics Material Library* as well as from [13–19].

	steel	molybdenum	air
density ρ [kg/m ³]	8.0 · 10 ³ ...7.7 · 10 ³	10.2 · 10 ³ ...9.7 · 10 ³	1.2...0.12
heat capacity c_p [(kg · K)]	485...746	244...562	1015...1306
thermal conductivity k [W/(m · K)]	13...25	139...84	2.6 · 10 ⁻² ...6.6 · 10 ⁻²
viscosity μ [Pa · s]	5.4 · 10 ⁻³ ...2.3 · 10 ⁻³	7.5 · 10 ⁻³ ...5.0 · 10 ⁻³	1.8 · 10 ⁻⁵ ...7.0 · 10 ⁻⁵
surface tension σ [N/m]	1.80...1.72	2.34...2.27	
absorption coefficient A [-]	0.31...0.27	0.27...0.34	
melting temperature T_m [K]	1810	2873	
evaporation temperature T_v [K]	3133	5833	
melting enthalpy H_m [J/kg]	2.8 · 10 ⁶	2.9 · 10 ⁶	
evaporation enthalpy H_v [J/kg]	6.1 · 10 ⁶	5.6 · 10 ⁶	

Table 1. Temperature dependent material data (blue: low temperature regime, red: high temperature regime)

Outside the temperature range available in literature material properties were assumed to be constant. The applied material properties are listed in Table 1.

Typical computation times for a molten track of $s = 360 \mu\text{m}$ were found to be in on the scale of 12 h on 4 cores of a dual CPU Intel Xeon E5-2630 v2 Dell Precision T5610 workstation.

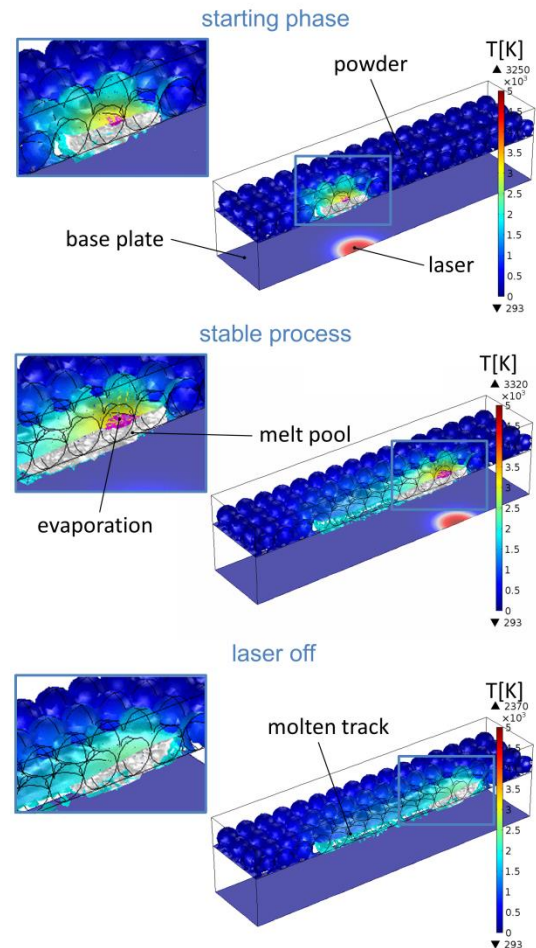


Figure 5. Selective Laser Melting of steel.

Simulation results at different process stages for SLM of steel and molybdenum at standard parameters for volume buildup for the respective material are shown in Figures 5 and 6. A comparison of the results makes obvious that SLM of steel and molybdenum operate in different process regimes. Whereas for steel a long melt pool is observed and evaporation plays a significant role, for molybdenum the melt pool size is restricted to the focal spot area and

temperatures are far below evaporation temperature. This has its origin in the different phase transition temperatures and thermal conductivities of the two materials. In SLM of molybdenum due to the high thermal conductivity of molybdenum heat losses are significantly higher, restricting the size of the melt pool. Besides that, the high heat losses in combination with the high evaporation temperature of molybdenum prevent the occurrence of evaporation.

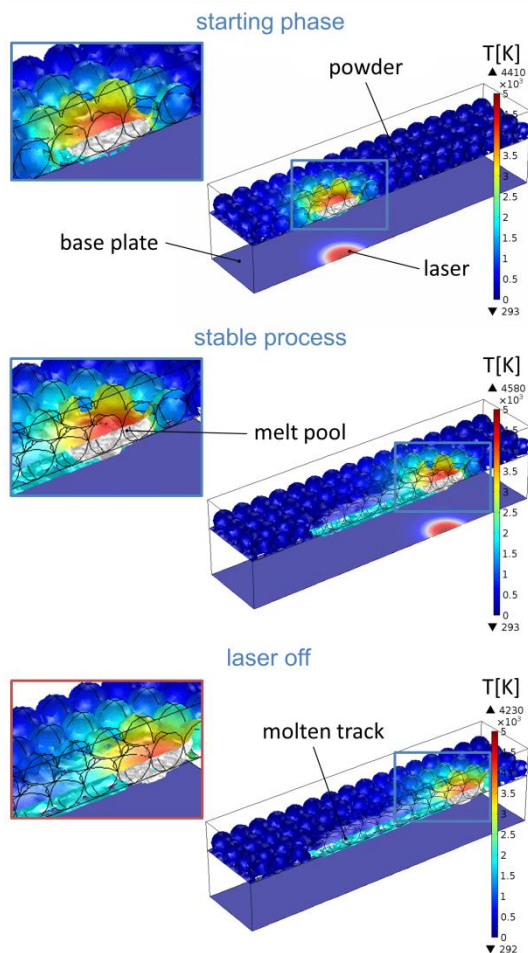


Figure 6. Selective Laser Melting of molybdenum.

More extended results obtained with the simulation model on the influence of process parameters in line and layer buildup from steel and molybdenum including experimental verification of the simulation model based on line width and surface roughness analyses have been published in [20-22].

4. Conclusions

The presented results demonstrate that the coupled thermo-fluidodynamical simulation model is able to describe the process dynamics of SLM as well as the material specific process characteristics. As the core of the model is the description of the laser beam-matter interaction, its applicability is not restricted to SLM. It can easily be adopted for a simulation of other laser based manufacturing processes.

5. References

- [1] R. Schiffler, Additive Schichtarbeit zwischen gestern und morgen, *VDI Nachrichten*, **15**, 22 (2015)
- [2] M. Geiger, K.-H. Leitz, H. Koch, A. Otto, A 3D transient model of keyhole and melt pool dynamics in laser beam welding applied to the joining of zinc coated sheets, *Production Engineering*, **3**, 127-136 (2009)
- [3] A. Otto, H. Koch, K.-H. Leitz, M. Schmidt, Numerical Simulations – A Versatile Approach for Better Understanding Dynamics in Laser Material Processing, *Physics Procedia*, **12**, 11-20 (2011)
- [4] K.-H. Leitz, H. Koch, A. Otto, M. Schmidt, Numerical simulation of process dynamics during laser beam drilling with short pulses, *Applied Physics A*, **106**, 885-891 (2012)
- [5] K.-H. Leitz, Mikro- und Nanostrukturierung mit kurz und ultrakurz gepulster Laserstrahlung, Meisenbach Verlag (2013) – ISBN 978-3-87525-355-9
- [6] M. Courtois, M. Carin, P. Le Masson, S. Gaied, M. Balabane, A complete model of keyhole and melt pool dynamics to analyze instabilities and collapse during laser welding, *Journal of Laser Applications*, **26**, 042001 (2014)
- [7] F.-J. Gürtler, M. Karg, K.-H. Leitz, M. Schmidt: Simulation of laser beam melting of steel powders using the three-dimensional volume of fluid method, *Physics Procedia*, **41**, 874-879 (2013)

- [8] S. A. Khairallah, A.T. Anderson, A. Rubenchik, W.E. King, Laser powder-bed fusion additive manufacturing: Physics of complex melt flow and formation mechanisms of pores, spatter and denudation zones, *Acta Materialia*, **108**, 36-45 (2016)
- [9] A.V. Gusarov, I. Smurov, Gas-dynamic boundary conditions of evaporation and condensation: Numerical analysis of the Knudsen layer, *Physics of Fluids*, Vol. **12**, Number 12, 4242-4255 (2002)
- [10] W. Demtröder, *Experimentalphysik 1 – Mechanik und Wärme*, Springer Verlag (2006) – ISBN 3-540-26034-X
- [11] H. Hügel, F. Dausinger, Fundamentals of laser-induced processes, *Landolt-Börnstein*, Volume **VIII/1C**, 3-68 (2004)
- [12] Y. Sun, C. Beckermann, Diffuse interface modeling of two-phase flows based on averaging: mass and momentum equations, *Physica D*, **198**, 281-308 (2004)
- [13] C.J. Smithells, *Metals Reference Book*. Butterworth, Fourth Edition (1967)
- [14] H. Stöcker, *Taschenbuch der Physik*. Harri Deutsch Verlag, 4. Auflage (2000) – ISBN 3-8171-1628-4
- [15] P.-F. Paradis, T. Ishikawa, N. Koike, Non-contact measurements of the surface tension and viscosity of molybdenum using an electrostatic levitation furnace, *International Journal of Refractory Metals & Hard Materials*, **25**, 95-100 (2007)
- [16] *Landolt-Börnstein – Zahlenwerte und Funktionen*, Springer Verlag (1963)
- [17] W.D. Wood, H.W. Deem, C.F. Lucks, *Handbook of High-Temperature Materials – Thermal Radiative Properties*, Plenum Press (1964)
- [18] M.J. Assael, K. Kakosimos, R.M. Banish, J. Brillo, I. Egry, R. Brooks, P.N. Quested, K.C. Mills, A. Nagashima, Y. Sato, W.A. Wakeham, Reference Data for the Density and Viscosity of Liquid Aluminum and Liquid Iron, *J. Phys. Chem. Ref. Data*, Vol. **35**, No.1, 285-300 (2006)
- [19] R.F. Brooks, I. Egry, S. Seetharaman, D. Grant, Reliable data for high-temperature viscosity and surface tension: results from a European project, *ECTP Proceedings*, 631-637 (2001)
- [20] K.-H. Leitz, P. Singer, A. Plankensteiner, B. Tabernig, H. Kestler, L.S. Sigl, Multi-Physical Simulation of Selective Laser Melting of Molybdenum, *Proceedings of Euro PM2015*, 4-7 October 2015, Reims, France (2015)
- [21] K.-H. Leitz, P. Singer, A. Plankensteiner, B. Tabernig, H. Kestler, L.S. Sigl, Multi-Physical Simulation of Selective Laser Melting, *Metal Powder Report* (2016) - in press
- [22] K.-H. Leitz, P. Singer, A. Plankensteiner, B. Tabernig, H. Kestler, L.S. Sigl, Thermo-Fluidodynamical Simulation of Layer Buildup by Selective Laser Melting of Molybdenum and Steel, *Proceedings of the MAMC 2016*, 24-25 November 2016, Linz, Austria (2016) - in press